Dynamic Depolarized Light Scattering and Nuclear Magnetic Relaxation Studies of Oligo- and Poly(methyl methacrylate)s in Dilute Solution

Yoshio Takaeda, Takenao Yoshizaki, and Hiromi Yamakawa*

Department of Polymer Chemistry, Kyoto University, Kyoto 606-01, Japan

Received August 5, 1994; Revised Manuscript Received October 22, 1994®

ABSTRACT: The (excess) power spectrum J_Γ of the depolarized component of scattered light was measured for 13 samples of atactic oligo- and poly(methyl methacylate)s (a-PMMA), each with the fraction of racemic diads $f_r = 0.79$, in the range of weight-average molecular weight M_w from 3.02×10^2 (trimer) to 7.55×10^3 in acetonitrile at 44.0 °C (Θ) and also for methyl isobutyrate in acetonitrile at 44.0 °C and in carbon tetrachloride at 25.0 °C. The spin–lattice relaxation time T_1 was also determined for the trimer through pentamer and the two samples with $M_w = 7.55 \times 10^3$ and 2.02×10^4, and the nuclear Overhauser enhancement NOE, for the trimer and the latter two samples, all in acetonitrile at 44 °C. It is found that, as in the case of atactic polystyrene (a-PS) previously studied, J_Γ may be well represented in terms of a single Lorentzian independently of M_w and that the relaxation time τ_Γ as defined as the reciprocal of the half-width at half-maximum of J_Γ evaluated at infinite dilution increases with increasing M_w and levels off to its asymptotic value in the limit of $M_w \to \infty$, being consistent with the recent theoretical prediction on the basis of the helical wormlike (HW) chain model. A comparison is made of the present data for τ_Γ, T_1, and NOE with the HW theory, and it is shown that the theory may explain satisfactorily the data in the range of $M_w \gtrsim 10^3$, although semiquantitatively for τ_Γ. For $M_w \lesssim 10^3$, the rigid sphere model having the radius equal to the apparent root-mean-square radius of gyration of the HW chain may give a good explanation of τ_Γ but not of T_1, indicating that the dynamic depolarized light scattering and nuclear magnetic relaxation cannot be described in terms of a common single relaxation time. However, there is shown to be an effective (mean) magnetic relaxation time τ_M which is approximately equal to $0.6\tau_\Gamma$. From a comparison of the present results for τ_Γ for a-PMMA with the previous ones for a-PS, the dynamic chain stiffness, as defined as the ratio of the relaxation time associated with the local motion of a long polymer chain to that of its isolated repeat unit (monomer), is found to be larger for a-PMMA than for a-PS, and it is shown that this difference may be well explained by the HW theory.

Introduction

In a previous paper,[1] we have started an experimental study of local motions of (unperturbed) flexible polymer chains in dilute solution, carrying out dynamic depolarized light scattering (LS) and nuclear magnetic relaxation measurements on solutions of atactic oligo- and polystyrene (a-PS) as a first typical example of flexible polymers. The relevant dynamic properties investigated are the spectrum J_Γ of the (excess) depolarized scattered component and the spin–lattice relaxation time T_1 along with the nuclear Overhauser enhancement NOE, respectively. All of these properties may be expressed in terms of the same class of basic time-correlation functions within the framework of the dynamic theory[2] of the helical wormlike (HW) chain,[2,3] and therefore we have made a combined analysis of the data obtained for them. The conclusions thus arrived at are the following. First, the results for J_Γ may be well represented in terms of a single Lorentzian independently of the molecular weight M and the relaxation time τ_Γ as defined as the reciprocal of the half-width at half-maximum of J_Γ levels off to its asymptotic value in the limit of $M \to \infty$, being consistent with the HW theoretical prediction.[4] Second, T_1 and NOE are closely correlated with τ_Γ. Third, the dynamic HW theories[4–6] may explain quantitatively the dependences on M of these properties except for NOE for $M \gtrsim 10^3$, while the rigid sphere model is valid for smaller M.

Thus, in the present paper, we proceed to make a study of these dynamic properties for atactic poly(methyl methacrylate) (a-PMMA) as another example of flexible polymers in the same fashion as in the previous paper[1] and compare the results with the previous ones for a-PS in order to provide a deeper understanding of the correlation between the local chain motions and conformations.

Now, in a series of experimental studies of equilibrium and steady-state transport properties of oligomers and polymers in the unperturbed (Θ) state,[7] it has already been shown that the value of the static stiffness parameter λ^{-1} of the HW model determined for a-PMMA (45.0–60.0 Å)[8–10] is appreciably larger than that for a-PS (20.6 Å).[11] On the other hand, an analysis based on the (dynamic) HW theory[6] has led to the conclusion that the dynamic chain stiffness, as defined as the ratio of the relaxation time associated with the local motion of a polymer chain to that of its isolated monomer unit, is larger for the chain with larger λ^{-1}. The value of τ_Γ for a-PMMA may then be expected to be larger than that for a-PS. One of the purposes of the present study is to examine whether this is true or not.

In the present study, almost all dynamic depolarized LS measurements have been carried out in acetonitrile at 44.0 °C (Θ). This requires some preliminary remarks, which concern a determination of the excess spectrum J_Γ for a-PMMA in this solvent. In the previous case of a-PS in cyclohexane or carbon tetrachloride,[1] the optical anisotropy of the solvent is negligibly small compared to that of the solute. Thus the spectrum of the depolarized component obtained for the solution by the use of a Fabry–Perot (FP) interferometer could easily be decomposed into J_Γ and the contribution from the solvent, the latter being only a flat base with a negligibly small amplitude. In the present case, however, the optical anisotropy of acetonitrile is larger than that of

® Abstract published in *Advance ACS Abstracts,* January 1, 1995.

0024-9297/95/2228-0682$09.00/0

Table 1. Values of M_w, x_w, and M_w/M_n for Atactic Oligo- and Poly(methyl methacrylate)s

sample	M_w	x_w	M_w/M_n
MIB	1.02×10^2		
OM3[a]	3.02×10^2	3	1.00
OM4	4.02×10^2	4	1.00
OM5	5.02×10^2	5	1.00
OM6a[b]	5.94×10^2	5.92	1.00
OM7	7.09×10^2	7.07	1.00
OM8a	7.93×10^2	7.91	1.01
OM12	1.16×10^3	11.6	1.02
OM15	1.50×10^3	15.0	1.03
OM18a	1.83×10^3	18.3	1.05
OM22	2.23×10^3	22.3	1.06
OM30	2.95×10^3	29.5	1.06
OM42	4.18×10^3	41.8	1.09
OM76	7.55×10^3	75.5	1.08
MM2a	2.02×10^4	202	1.08

[a] M_w's of OM3 through OM5 and OM7 had been determined by analytical GPC.[8] [b] M_w's of OM6a and OM8a through MM2a had been determined from LS measurements in acetone at 25.0 °C.[8,13,14]

a-PMMA,[12] so that we have taken into account the FP spectrum of the solvent by the use of a procedure devised to determine J_Γ accurately. For the confirmation of the accuracy of this procedure, it is desirable to carry out measurements also in a solvent with small optical anisotropy, e.g., carbon tetrachloride, and to compare the results with those in acetonitrile. Unfortunately, however, it is known that the exposure of the solution of a-PMMA in carbon tetrachloride to a strong laser beam denatures (precious) a-PMMA samples.[12] Thus, such an examination has been restricted to the monomer of PMMA, i.e., methyl isobutyrate.

Experimental Section

Materials. All the samples used in this work are the same as those used in the previous studies of the mean-square radius of gyration and the intrinsic viscosity (in Θ and good solvents),[8,9,13] the mean-square optical anisotropy,[12] the translational diffusion coefficient,[10] and the second virial coefficient.[14] They are the fractions separated by preparative gel permeation chromatography (GPC) or fractional precipitation from the original samples prepared by group-transfer polymerization and have a fixed stereochemical composition (the fraction of racemic diads $f_r = 0.79$) independent of M, possessing hydrogen atoms at both ends of the chain. Methyl isobutyrate (MIB) (Tokyo Kasei Kogyo Co.; 99.0% purity), the monomer of PMMA, was purified by distillation after dehydration by passing through a silica gel column. The values of the weight-average molecular weight M_w, the weight-average degree of polymerization x_w, and the ratio of M_w to the number-average molecular weight M_n are listed in Table 1. As seen from the values of M_w/M_n, all the samples are sufficiently narrow in molecular weight distribution, and, in particular, the samples OM3 through OM5 are completely monodisperse.

The solvents acetonitrile and carbon tetrachloride (CCl_4) were purified according to standard procedures prior to use.

Dynamic Depolarized Light Scattering. The photometer used for all dynamic depolarized LS measurements is the same as that used in the previous studies,[1,12,15] i.e., a Brookhaven Instruments Model BI-200SM goniometer with a minor modification of its light source part and with a detector alignment newly assembled to incorporate a Fabry–Perot (FP) interferometer in it. It has been described in detail in the previous paper,[12] and therefore we here only give its short sketch.

Vertically polarized light of wavelength 488 nm from a Spectra-Physics Model 2020 argon ion laser equipped with a Model 583 temperature-stabilized etalon for single-frequency-mode operation was used as a light source. It was made highly vertically (v) polarized by passing through a Glan–Thompson (GT) prism with an extinction ratio smaller than 10^{-5}. The scattered light was measured at a scattering angle of 90°. Its horizontal (H) component, i.e., the depolarized (Hv) component, which was extracted from the total scattered light intensity by the use of the same GT prism as above, was analyzed with a Burleigh Instruments Model RC-110 FP interferometer equipped with a Model RC-670 pair of plane mirrors with a flatness of $\lambda/200$ and a reflectivity of 97.5%. The intensity of the Hv components filtered through the FP interferometer was measured by an EMI 9893B/350 photomultiplier (PM) tube. As in the previous study,[1] we used a pinhole of diameter 25 μm as a spatial filter, which was placed between the interferometer and the PM tube. All the measurements were carried out by the single passing as in the previous study.[1]

As before,[1,15] the transmittance $T(\omega)$ was determined by measuring the polarized component of the light scattered from a solution of an a-PS sample with $M_w = 7.32 \times 10^5$ in methyl ethyl ketone at the concentration $c \simeq 1 \times 10^{-3}$ g/cm^3 and at 25.0 or 44.0 °C, following Ouano and Pecora.[16]

In the present study, the free spectral range (FSR) of the interferometer (i.e., the distance between the mirrors) was changed from 4.7×10^{10} to 3.0×10^{13} rad/s, depending on the width of J_Γ, in order to attain an appropriate resolution. As in the previous study,[1] the value δ of FSR for each setting was determined by the use of the sodium doublet of separation 0.597 nm at 589.3 nm for $\delta \gtrsim 5 \times 10^{12}$ rad/s, of the ^{4}He hyperfine structure interval of 1.0 cm^{-1} at 587.5 nm associated with the 2^3P-3^3D transition for $4 \times 10^{11} \lesssim \delta \lesssim 2 \times 10^{12}$ rad/s, and of the Brillouin shift $\Delta\omega_B$ of 3.53×10^{10} rad/s in the Rayleigh–Brillouin spectrum of pure benzene at 25.0 °C at 1 atm for $10^{11} \lesssim \delta \lesssim 3 \times 10^{11}$ rad/s. For $\delta \lesssim 10^{11}$ rad/s, the distance between the mirrors was directly measured.

Measurements were carried out on solutions of all the samples except for MM2a in acetonitrile at 44.0 °C (Θ) and on those of MIB in CCl_4 at 25.0 °C. The most concentrated solutions of each sample were prepared gravimetrically and made homogeneous by continuous stirring at ca. 50 °C for 1–3 days in acetonitrile and for 1 day in CCl_4. These solutions and solvents were optically purified by filtration through a Teflon membrane of pore size 0.1 or 0.45 μm. The solutions of lower concentrations were obtained by successive dilution. The weight concentrations of the test solutions were converted to the solute mass concentrations c (in g/cm^3) by the use of the densities of the solutions.

Before and after each measurement on the solution or solvent, the transmittance of the FP interferometer was determined in the manner as described above. In the present measurements, the finesse could be kept at 50–60 during a single measurement, which took ca. 40 min for both cases.

Nuclear Magnetic Relaxation. T_1 of ^{13}C was determined for aliphatic carbon atoms of the samples OM3, OM4, OM5, OM76, and MM2a by the inversion–recovery method with a pulse sequence $\pi-t-\pi/2$ on a JEOL JNM GX-400 spectrometer at 100.4 MHz. NOE for each of those carbon atoms of the samples OM3, OM76, and MM2a was evaluated from the ratio of the integrated intensity of its peak obtained with complete noise decoupling of protons to that obtained with gated decoupling only during data acquisition. A pulse delay was taken to be longer than 5 times as long as the largest T_1 of aliphatic carbon atoms under observation. Measurements were carried out on solutions in acetonitrile at 44 °C with a lock signal obtained from an external C_6D_{12} tube. The solutions were not degassed since T_1's of interest rarely exceeded 2 s, as shown later.

Results

Depolarized Spectrum J_Γ. As mentioned in the Introduction, the optical anisotropy of the solute, a-PMMA, is much smaller than that of a-PS studied in the previous paper,[1] and moreover, that of the solvent, acetonitrile, is very large compared to those of the isotropic solvents for the latter, cyclohexane and CCl_4.[1] Then, for a-PMMA in acetonitrile, the contribution of the solvent to the spectrum I_{Hv} of the Hv component of light scattered from the solution is too large to neglect.[12]

We must therefore subtract it from I_{Hv} to evaluate the excess spectrum ΔI_{Hv} due to the solute. For this purpose, it is necessary to examine the spectrum $I_{Hv,solv}$ itself of the Hv component of light scattered from the pure solvent. We note that this is also the case even with solutions of MIB in CCl_4,[12] although the contribution of the solvent is much smaller than that in the case of acetonitrile.

Before proceeding to make the above examination, it is convenient here to give a brief description of the FP interferometer and the (apparent) spectrum I_{ap} obtained by the use of it. It is a periodic filter such that its transmittance $T(\omega)$ is a periodic function of angular frequency ω of light passing through it with period δ (the value of the FSR).[17] In the present case of the single passing, $T(\omega)$ may be well represented by a sum of Lorentzians as

$$T(\omega) \simeq \sum_{j=0}^{\infty} T_j(\omega) \tag{1}$$

with

$$T_j(\omega) = T_{max}[1 + (2F/\delta)^2(\omega - j\delta)^2]^{-1} \tag{2}$$

where T_{max} is the maximum transmittance and F is the finesse to be determined experimentally as mentioned in the Experimental Section. Note that F is equal to the ratio of δ to the full-width at half-maximum (fwhm) of the transmittance curve, and therefore represents the resolution of the interferometer, and also that the jth peak of the transmittance is located at $\omega = j\delta$.

Consider a scattered light beam whose (true) spectrum is given by $I(\Delta\omega)$ as a function of the difference $\Delta\omega$ between the angular frequencies of the scattered light and incident light waves, the latter being designated by ω_0. Then the spectrum $I_{ap}(\Delta\omega_{ap})$ observed with the FP interferometer as a function of the difference $\Delta\omega_{ap}$ between ω_0 and the angular frequency of the transmittance peak closest to ω_0 may be written in the form[15]

$$I_{ap}(\Delta\omega_{ap}) = \sum_{j=-n+1}^{n-1} \int_{-(n-1/2)\delta}^{(n-1/2)\delta} T_j(\Delta\omega - \Delta\omega_{ap})\, I(\Delta\omega)\, d(\Delta\omega) \tag{3}$$

where n is a proper positive integer such that $I(\Delta\omega)$ is negligibly small for $|\Delta\omega| > (n - 1/2)\delta$. If δ is (experimentally) chosen to be sufficiently larger than the width of $I(\Delta\omega)$, then n may be set equal to unity.

The use of eq 3 requires some further remarks. In general, the spectrum I_{Hv} for a solution is composed of those associated with the solute and solvent, and their widths are proportional to the reciprocals of the rotatory relaxation times of the scattering unit in the solute polymer chain and the solvent molecule, respectively. As the polymer molecular weight M_w is increased, the former relaxation time increases, and the width of its spectrum becomes narrower and narrower than that of the latter. In the previous measurements on a-PS,[1] the contribution of the solvent (cyclohexane or CCl_4) could be neglected compared to that of the solute a-PS, so that I_{Hv} could be considered to be identical with the excess spectrum ΔI_{Hv}, i.e., the spectrum associated with a-PS. In such cases, we could always choose those values of δ which satisfy the two conditions that the width of I_{Hv} is sufficiently smaller than δ and that it is sufficiently larger than the fwhm of the transmittance curve. (In particular, the second condition is necessary for an accurate determination of the spectrum.) The true spectrum $I(\Delta\omega)$ could then be evaluated with sufficient accuracy by solving the integral equation 3 with $n = 1$.

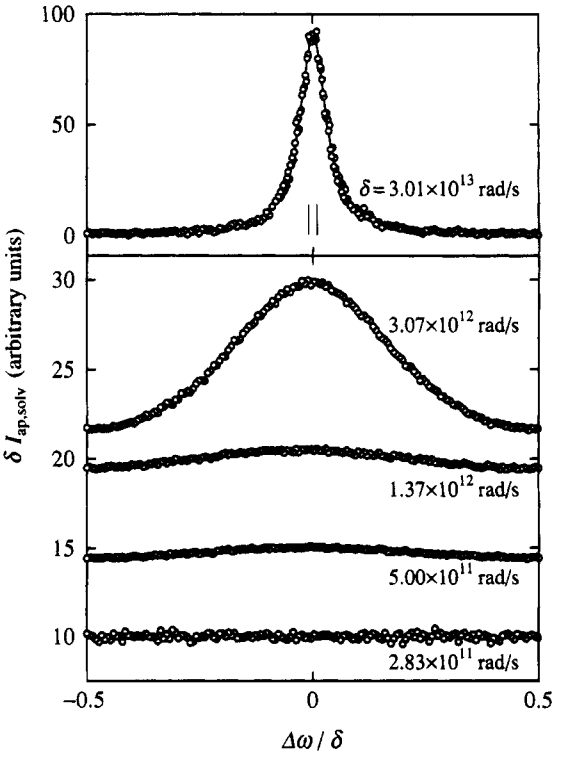

Figure 1. Plots of $\delta I_{ap,solv}$ against $\Delta\omega/\delta$ for (pure) acetonitrile at 44.0 °C obtained for various values of δ indicated. The data points for $\delta = 5.00 \times 10^{11}$, 1.37×10^{12}, and 3.07×10^{12} rad/s are shifted upward by 5, 10, and 15 (in the indicated units), respectively. The solid curves represent the values of the respective best-fit Lorentzians (see text). A pair of vertical line segments indicate the resolution of the interferometer for $\delta = 3.01 \times 10^{13}$ rad/s.

Unfortunately, however, this is not the case with solutions of a-PMMA in acetonitrile, for which the contribution of the solvent must be taken into account. For such solutions, we have not always been able to find those values of δ which satisfy the above two conditions for both constituent spectra for the solute and solvent. Therefore, we choose those values of δ which satisfy the two conditions only for the former spectrum. In anticipation of the results, we note that the values of δ thus chosen are the following, depending on M_w: 3.01×10^{13} rad/s for MIB, 3.07×10^{12} rad/s for the samples OM3 and OM4, 1.37×10^{12} rad/s for the samples OM5 and OM6a, 5.00×10^{11} rad/s for the samples OM7 and OM8a, 2.83×10^{11} rad/s for the sample OM12, and so on. Of course, these values of δ cannot generally satisfy the first condition above for the latter spectrum, so that we need eq 3 with $n > 1$ as the expression for $I_{ap}(\Delta\omega_{ap})$ for the solvent.

Now, we proceed to examine the spectra $I_{ap,solv}(\Delta\omega)$ of the Hv component of light scattered from the pure solvent acetonitrile. Figure 1 shows $I_{ap,solv}(\Delta\omega)$ (multiplied by δ) plotted against $\Delta\omega/\delta$ for acetonitrile at 44.0 °C for the above five values of δ. Here and hereafter, the subscripts ap on $\Delta\omega$ and Hv on I and ΔI are omitted, for simplicity. All the spectra have been properly normalized so that their total intensities may be identical with each other, and the spectra measured with $\delta = 5.00 \times 10^{11}$, 1.37×10^{12}, and 3.07×10^{12} rad/s have been shifted upward by 5, 10, and 15 (in the indicated

units), respectively. In the figure, a pair of vertical line segments indicate the resolution of the FP interferometer; their interval is equal to $1/F$, i.e., the fwhm of the transmittance curve divided by δ, which was determined prior to the measurement of $I_{ap,solv}$ with $\delta = 3.01 \times 10^{13}$ rad/s. Although we have not indicated such resolutions for the spectra with $\delta \leq 3.07 \times 10^{12}$ rad/s, they are almost the same as that for the case of $\delta = 3.01 \times 10^{13}$ rad/s since F is almost constant for all measurements, as mentioned in the Experimental Section. It is seen from the spectrum for $\delta = 3.01 \times 10^{13}$ rad/s that this value of δ, which has been chosen to satisfy the above two conditions for the solute MIB, also satisfies them for the solvent acetonitrile. (Note that the width of the apparent spectrum is larger than the true one). This is rather natural, considering the fact that the rotatory relaxation time of the solvent molecule is of the same order of magnitude as that of MIB. As δ is decreased, the spectrum becomes broader and its peak vanishes completely for $\delta = 2.83 \times 10^{11}$ rad/s. Thus, for $\delta \leq 2.83 \times 10^{11}$ rad/s, the contribution of the solvent may be treated as a flat base, so that the spectrum ΔI associated with the solute may be evaluated in the same manner as in the previous paper.[1] For larger δ, we evaluate ΔI as follows.

The apparent spectrum $I_{ap}(\Delta\omega)$ for a solution may be written in the form

$$I_{ap}(\Delta\omega) = \Delta I_{ap}(\Delta\omega) + I_{ap,solv}(\Delta\omega) \quad (4)$$

where $\Delta I_{ap}(\Delta\omega)$ is the apparent excess spectrum for the solute and $I_{ap,solv}(\Delta\omega)$ is the corresponding apparent spectrum for the solvent for an appropriate value of δ shown in Figure 1. It must be noted that the constituent spectrum for the solvent in the solution may possibly be somewhat altered from the one for the pure solvent by an addition of the solute molecules as in the case of solutions of poly(dimethylsiloxane) in bromocyclohexane.[15] However, such a deviation of the spectrum for the solvent must be very small in dilute solution and vanish completely at infinite dilution. Thus we may evaluate ΔI_{ap} (or ΔI) from eq 4 with the values of I_{ap} and $I_{ap,solv}$ determined for the solution and pure solvent. Then the use of the observed $I_{ap,solv}(\Delta\omega)$ itself introduces additional statistical errors, and therefore we replace it by a smoothed function.

We first consider this smoothing. For the four $I_{ap,solv}(\Delta\omega)$ for $\delta \geq 5.00 \times 10^{11}$ rad/s shown in Figure 1, it has been found (as a result of the solution of eq 3) that their true spectra $I_{solv}(\Delta\omega)$ may be represented by a single Lorentzian in a good approximation, so that $I_{ap,solv}(\Delta\omega)$ may be given by eq 3 (with $I_{ap,solv}$ in place of I_{ap}) with eq 2 and with a proper value of n, where I_{solv} (in place of I) is given by

$$I_{solv}(\Delta\omega) = (A_{solv}c_{solv}/\pi)[1 + (c_{solv}\Delta\omega)^2]^{-1} \quad (5)$$

In eq 5, the coefficients A_{solv} and c_{solv} are adjustable parameters and have been determined so that the sum f_{solv} of residual errors defined by

$$f_{solv}(A_{solv},c_{solv}) = \sum_{i=1}^{N} |I_{ap,solv,i} - I_{ap,solv}(\Delta\omega_i)|^2 \quad (6)$$

may be minimized, where $I_{ap,solv,i}$ is the (apparent) intensity observed at $\Delta\omega = \Delta\omega_i$ and $I_{ap,solv}(\Delta\omega_i)$ is the (apparent) intensity calculated from eq 3 with eqs 2 and 5 (with proper values of parameters). The values of n used and those of c_{solv} thus determined are $n = 1$ and $c_{solv} = 1.25 \times 10^{-12}$ s for $\delta = 3.01 \times 10^{13}$ rad/s, $n = 2$ and $c_{solv} = 1.25 \times 10^{-12}$ s for $\delta = 3.07 \times 10^{12}$ rad/s, $n = 3$ and $c_{solv} = 1.23 \times 10^{-12}$ s for $\delta = 1.37 \times 10^{12}$ rad/s, and $n = 3$ and $c_{solv} = 1.27 \times 10^{-12}$ s for $\delta = 5.00 \times 10^{11}$ rad/s. The values of A_{solv} thus determined are not used for later developments and therefore are not given here. We note that the coefficient c_{solv} corresponds to the (single) rotatory relaxation time of the solvent molecules and must therefore be independent of δ. Indeed, this is seen to be the case approximately. The values of $I_{ap,solv}(\Delta\omega)$ (best-fitted to the data) for $\delta \geq 5.00 \times 10^{11}$ rad/s calculated from eq 3 with eqs 2 and 5 and with the values of n and c_{solv} given above are also represented in Figure 1 by the solid curves, although those for $\delta \leq 3.07 \times 10^{12}$ rad/s are invisible behind the data points. It is seen that the best-fit values may reproduce well the observed ones. Thus, for $\delta \geq 5.00 \times 10^{11}$ rad/s, we adopt eq 3 with eqs 2 and 5 and with the values of n and c_{solv} determined above as the expression for the smoothed function $I_{ap,solv}(\Delta\omega)$, where the coefficient A_{solv} (dependent on δ) is treated as a readjustable parameter. For $\delta \leq 2.83 \times 10^{11}$ rad/s, $I_{ap,solv}(\Delta\omega)$ may be considered to be a constant, as mentioned above, and therefore we may put

$$I_{ap,solv}(\Delta\omega) = A_{solv} \quad \text{for } \delta \leq 2.83 \times 10^{11} \text{ rad/s} \quad (7)$$

where this A_{solv} is also an adjustable parameter. Note that for such small δ, this is equivalent to $n \to \infty$.

Now we evaluate the desired $\Delta I(\Delta\omega)$ by the use of the smoothed function introduced above. As in the previous study of a-PS,[1] we express $\Delta I(\Delta\omega)$ as a sum of several normalized Lorentzians, i.e.,

$$\Delta I(\Delta\omega) = \sum_{i=1}^{m} (A_i c_i/\pi)[1 + (c_i\Delta\omega)^2]^{-1} \quad (8)$$

where $(A_1, A_2, ..., A_m) = \{A_m\}$ and $(c_1, c_2, ..., c_m) = \{c_m\}$ are adjustable parameters. We note that in eq 8 we have omitted a constant term A_0, which had appeared in eq 5 of ref 1, since the amplitude of such a constant term is always negligibly small and its omission never causes appreciable effects on the results. Then, $I_{ap}(\Delta\omega)$ observed for a given solution for a given value of δ may be expressed by eq 4 with $\Delta I_{ap}(\Delta\omega)$ given by eq 3 (with ΔI_{ap} and ΔI in place of I_{ap} and I, respectively) with eq 8 and $n = 1$, i.e.,

$$\Delta I_{ap}(\Delta\omega) = \sum_{i=1}^{m} (A_i c_i/\pi) \int_{-\delta/2}^{\delta/2} T_0(\Delta\omega' - \Delta\omega) \times [1 + (c_i\Delta\omega')^2]^{-1} \, d(\Delta\omega') \quad (9)$$

and with $I_{ap,solv}(\Delta\omega)$ given by eq 3 (with $I_{ap,solv}$ and I_{solv} in place of I_{ap} and I, respectively) with eq 5 or by eq 7, i.e.,

$$I_{ap,solv}(\Delta\omega_{ap}) = (A_{solv}c_{solv}/\pi) \sum_{j=-n+1}^{n-1} \int_{-(n-1/2)\delta}^{(n-1/2)\delta} T_j(\Delta\omega' - \Delta\omega) \times [1 + (c_{solv}\Delta\omega')^2]^{-1} \, d(\Delta\omega') \quad \text{for } \delta \geq 5.00 \times 10^{11} \text{ rad/s}$$

$$= A_{solv} \quad \text{for } \delta \leq 2.83 \times 10^{11} \text{ rad/s} \quad (10)$$

where $T_j(\Delta\omega)$ is given by eq 2 and we use the values of

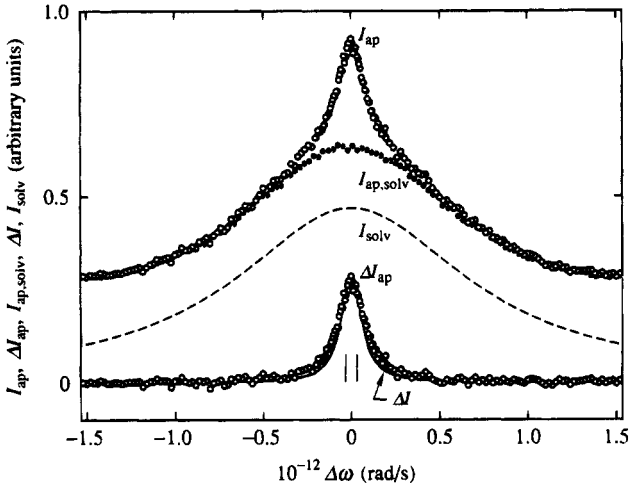

Figure 2. Plots of I_{ap}, ΔI_{ap}, $I_{ap,solv}$, ΔI, and I_{solv} against $\Delta\omega$ for sample OM3 in acetonitrile at 44.0 °C at $c = 0.100$ g/cm^3. A pair of vertical line segments indicate the resolution of the interferometer.

n and c_{solv} determined above. Thus we may evaluate $\Delta I(\Delta\omega)$ from eq 8 with the values of $\{A_m\}$ and $\{c_m\}$ determined (along with that of A_{solv}) so that the sum f of residual errors defined by

$$f(\{A_m\},\{c_m\},A_{solv}) = \sum_{i=1}^{N} |I_{ap,i} - I_{ap}(\Delta\omega_i)|^2 \quad (11)$$

may be minimized, where $I_{ap,i}$ is the (apparent) intensity observed at $\Delta\omega = \Delta\omega_i$ and $I_{ap}(\Delta\omega_i)$ is the (apparent) intensity calculated from eq 4 with eqs 9 and 10. In practice, we have put $m = 6$ in eq 9 and replaced the convolutions of the two Lorentzians on the right-hand sides of eqs 9 and 10 by the respective resultant single Lorentzians in a good approximation.

Figure 2 shows plots of I_{ap} (unfilled circles), ΔI (solid curve), and I_{solv} (dashed curve) obtained for a solution of the sample OM3 in acetonitrile at 44.0 °C at $c = 0.100$ g/cm^3. In the figure, the lower unfilled circles represent the values of ΔI_{ap}, which is not a direct observable, evaluated by subtracting the calculated values of $I_{ap,solv}$ (not shown) from the observed ones of I_{ap}, where the former values have been calculated from eq 10 with the values of n and c_{solv} given above for $\delta = 3.07 \times 10^{12}$ rad/s and with that of A_{solv} determined from the above fitting of the calculated values of ΔI_{ap} to the observed ones. There are also plotted the observed values of $I_{ap,solv}$ (filled circles) (shown in Figure 1) for $\delta = 3.07 \times 10^{12}$ rad/s, which have been renormalized so that its total intensity may be equal to that of the calculated $I_{ap,solv}$. A pair of vertical line segments in the figure indicate the resolution of the FP interferometers as in Figure 1. Here we have not shown the values of the calculated values of I_{ap}, ΔI_{ap}, and $I_{ap,solv}$, since they may reproduce completely the respective observed values and would be invisible behind the respective data points if they were plotted. It is seen that the plots of I_{ap} and (observed) $I_{ap,solv}$ completely agree with each other in the range $|\Delta\omega| \gtrsim 5 \times 10^{11}$ rad/s, so that ΔI_{ap} vanishes in this range. This confirms the validity of the above procedure for determining ΔI accurately. Therefore, $\Delta I(\Delta\omega)$ thus determined may be regarded as the desired depolarized spectrum $J_\Gamma(\Delta\omega)$ due to the solute a-PMMA.

Figure 3 shows spectra I_{ap} (unfilled circles), J_Γ (solid curve), and I_{solv} (dashed curve) obtained similarly for solutions of MIB and the sample OM5 in acetonitrile

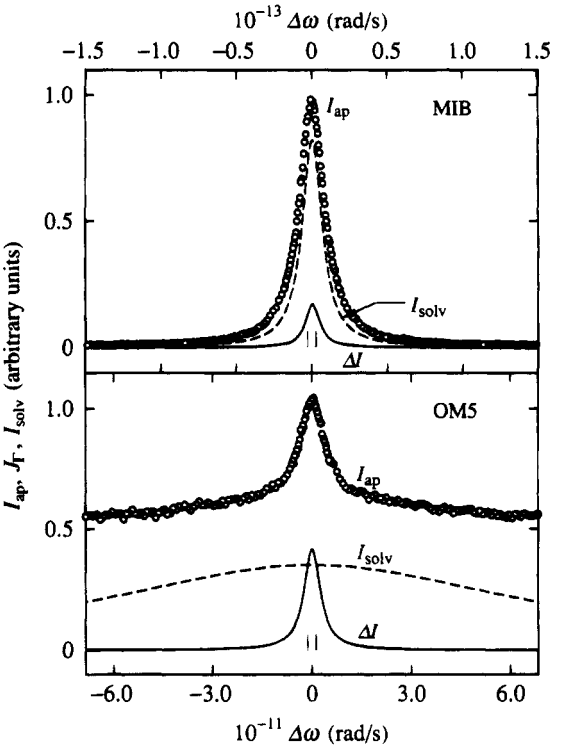

Figure 3. Plots of I_{ap}, J_Γ, and I_{solv} against $\Delta\omega$ for MIB and sample OM5 in acetonitrile at 44.0 °C at $c = 0.122$ and 0.101 g/cm^3, respectively. A pair of vertical line segments indicate the resolution of the interferometer.

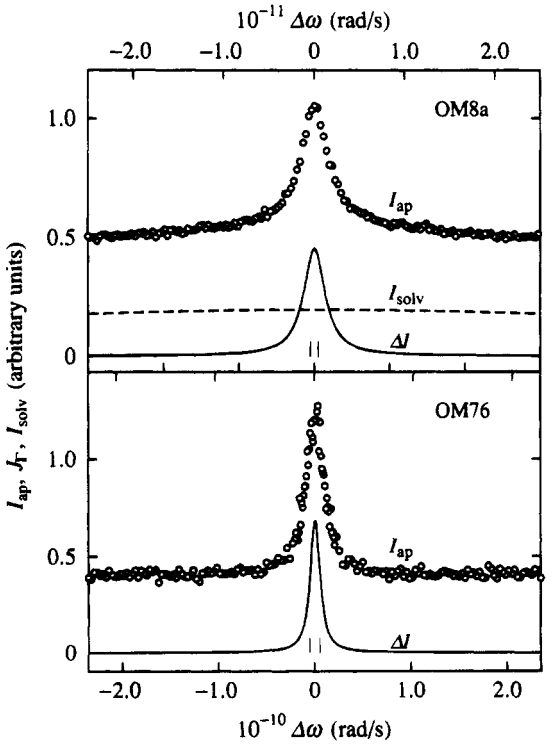

Figure 4. Plots of I_{ap}, J_Γ, and I_{solv} against $\Delta\omega$ for samples OM8a and OM76 in acetonitrile at 44.0 °C at $c = 0.112$ and 0.116 g/cm^3, respectively; see legend to Figure 3.

at 44.0 °C at $c = 0.122$ and 0.101 g/cm^3, respectively. A pair of vertical line segments have the same meaning as in Figure 2. Figure 4 shows similar plots for the samples OM8a and OM76 in acetonitrile at 44.0 °C at $c = 0.112$ and 0.116 g/cm^3, respectively, where I_{solv} has not been plotted for the sample OM76 since it cannot be evaluated for $\delta \leq 2.83 \times 10^{11}$ rad/s. It is interesting

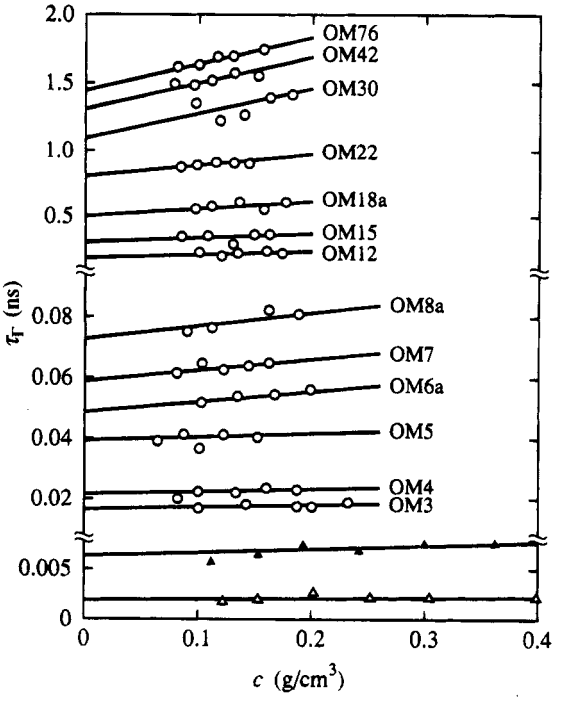

Figure 5. Plots of τ_Γ against c for all a-PMMA samples except for MM2a in acetonitrile at 44.0 °C. The unfilled and filled triangles represent the values for MIB in acetonitrile at 44.0 °C and in CCl_4 at 25.0 °C, respectively.

to note that, for all cases including those shown in Figures 2–4, the coefficients c_i (i = 1–6) of the six Lorentzians have been found to be the same, indicating that $J_\Gamma(\Delta\omega)$ may be fitted by a single Lorentzian as in the previous results for a-PS.[1] The present results for a-PMMA are therefore also consistent with our theory,[4] although it predicts that there is a minor contribution of another Lorentzian.

Relaxation Time τ_Γ. Now we consider the (apparent) relaxation time τ_Γ as defined as the reciprocal of the half-width at half-maximum (hwhm) of $J_\Gamma(\Delta\omega)$ thus determined, which is just the hwhm of the single Lorentzian in the present case. Figure 5 shows plots of τ_Γ against c for all a-PMMA samples except for MM2a in acetonitrile at 44.0 °C and also for MIB in CCl_4 at 25.0 °C. Each plot follows a straight line and the value of τ_Γ at infinite dilution may be evaluated from its intercept. As in the case of a-PS in cyclohexane at 34.5 °C and in CCl_4 at 25.0 °C previously studied,[1] τ_Γ is seen to increase with increasing c for all the samples.

The values of τ_Γ thus determined at infinite dilution are given in Table 2 along with those of $k_BT\tau_\Gamma/\eta_0$ with k_B the Boltzmann constant, T the absolute temperature, and η_0 the solvent viscosity. The latter values have been calculated from the former with the values 0.285 and 0.904 cP of η_0 for acetonitrile at 44.0 °C and for CCl_4 at 25.0 °C, respectively. As discussed in the previous paper,[1] the reduced relaxation time $k_BT\tau_\Gamma/\eta_0$ must be independent of solvent condition if the motions of the small molecules or the motional units in the polymer chain may be described in the diffusion limit and if the local chain conformation does not depend on that condition. Since the values of $k_BT\tau_\Gamma/\eta_0$ for MIB in the two solvents agree well with each other, the dynamics that governs τ_Γ may be considered to be described in this limit for solutions of a-PMMA in acetonitrile.

Figure 6 shows plots of $k_BT\tau_\Gamma/\eta_0$ at infinite dilution against the logarithm of M_w for a-PMMA in acetonitrile at 44.0 °C. The solid curve connects smoothly the data points for OM3 through OM76, and the dashed line segment connects those for MIB and OM3. (The vertical line segments attached to the data points indicate the limit of experimental error.) As in the case of a-PS,[1] the reduced relaxation time $k_BT\tau_\Gamma/\eta_0$ increases with increasing M_w and seems to level off in the limit of $M_w \to \infty$, being consistent with our theory.[4] Its asymptotic value in this limit is found to be ca. 2×10^4 Å^3, which is appreciably larger than the corresponding value 4×10^3 Å^3 previously obtained for a-PS.[1]

Table 2. Values of τ_Γ and $k_BT\tau_\Gamma/\eta_0$ for Atactic Oligo- and Poly(methyl methacrylate)s in Acetonitrile at 44.0 °C at Infinite Dilution

sample	τ_Γ, ns	$k_BT\tau_\Gamma/\eta_0$, Å^3
MIB	0.0019_3 (0.0063_0)[a]	$2.9_6 \times 10$ ($2.8_6 \times 10$)[a]
OM3	0.016_5	$2.5_3 \times 10^2$
OM4	0.021_6	$3.3_1 \times 10^2$
OM5	0.039_4	$6.0_5 \times 10^2$
OM6a	0.048_6	$7.4_7 \times 10^2$
OM7	0.058_8	$9.0_3 \times 10^2$
OM8a	0.072_8	$1.1_2 \times 10^3$
OM12	0.18_5	$2.8_4 \times 10^3$
OM15	0.30_5	$4.6_9 \times 10^3$
OM18a	0.50_0	$7.6_8 \times 10^3$
OM22	0.80_4	$1.2_4 \times 10^4$
OM30	1.0_9	$1.6_8 \times 10^4$
OM42	1.3_1	$2.0_1 \times 10^4$
OM76	1.4_4	$2.2_2 \times 10^4$

[a] The figures in parentheses represent the values in CCl_4 at 25.0 °C.

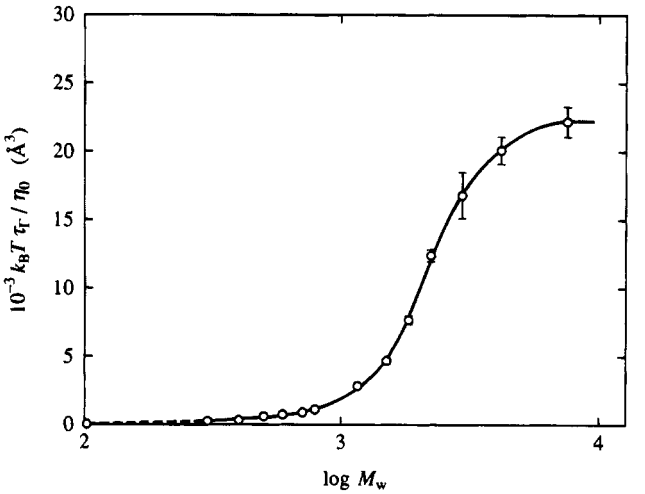

Figure 6. Plots of $k_BT\tau_\Gamma/\eta_0$ at infinite dilution against the logarithm of M_w for a-PMMA in acetonitrile at 44.0 °C. The solid curve connects smoothly the data points for OM3 through OM76, and the dashed line segment connects those for MIB and OM3.

Spin–Lattice Relaxation Time T_1 and Nuclear Overhauser Enhancement NOE. For a-PS previously studied,[1] the nuclear magnetic spins of all main-chain (aliphatic) ^{13}C atoms relax due to the dipolar interactions with bonded hydrogen atoms. For a-PMMA, on the other hand, the spins of the methylene ^{13}C atoms also relax by the same mechanism as above, but those of the α-^{13}C atoms do not since the latter have no bonded hydrogen atoms, so that we consider T_1 and NOE only of the methylene ^{13}C atoms. We note that the nuclear magnetic relaxation of its methyl ^{13}C atoms does not directly reflect local motions of its main chain, and is not considered, for simplicity.

The values of T_1 and NOE of the methylene ^{13}C atoms for the sample OM3 in acetonitrile at 44.0 °C are given in Table 3. As explicitly shown in its caption, the

Table 3. Values of $T_{1,\alpha}$ and NOE_α ($\alpha = m,r$) for OM3 in Acetonitrile at 44 °C

$$\overset{1}{H}CH_2CCH_3(X)\overset{2}{C}H_2CCH_3(X)\overset{3}{C}H_2CCH_3(X)H$$

(X = $COOCH_3$)

carbon atom no.	($T_{1,m}$, $T_{1,r}$), s		(NOE_m, NOE_r)
	c = 0.080 g/cm^3	c = 0.140 g/cm^3	c = 0.078 g/cm^3
2	(2.12, 2.02)	(2.00, 1.83)	(3.0, 2.9)
3	(2.09, 2.16)	(1.86, 1.99)	(3.1, 2.9)

Table 4. Values of $T_{1,\alpha\beta}$ ($\alpha,\beta = m,r$) for OM4 in Acetonitrile at 44 °C

$$\overset{1}{H}CH_2CCH_3(X)\overset{2}{C}H_2CCH_3(X)\overset{3}{C}H_2CCH_3(X)\overset{4}{C}H_2CCH_3(X)H$$

(X = $COOCH_3$)

carbon atom no.	($T_{1,mr}$, $T_{1,rm}$, $T_{1,rr}$), s	
	c = 0.090 g/cm^3	c = 0.148 g/cm^3
2	(1.25, 1.27, 1.25)	(1.19, 1.14, 1.19)
3	(1.37, 1.25, 1.26)	(1.29, 1.37, 1.13)
4	(1.26, 1.34, 1.26)	(1.14, 1.39, 1.14)

methylene carbon atoms have been numbered from the one in the initiating-end monomer group to the one in the terminating-end monomer group. Note that the carbon atom numbered 1 is not the methylene one but the methyl one since the initiating end of the a-PMMA samples used is a hydrogen atom. This numbering has been adopted for convenience of clarification of the position of the methylene carbon atom numbered i ($i \geq 2$) in the oligomer chain, and we consider T_1 and NOE of those with $i \geq 2$. The sample OM3 is a mixture of the two stereoisomers, i.e., meso (m) and racemic (r), so that each ^{13}C has two absorption peaks. Then, for OM3, the number of peaks that we are interested in is four. We have identified each peak of the ^{13}C NMR spectra by the use of the assignments previously determined for the same sample.[18] We note that, although we could not estimate the experimental errors in the raw data, the errors in the evaluation of T_1 from the spectra are at most ca. ±2%. It is seen that the values of NOE obtained for the sample OM3 are ca. 3 for all ^{13}C atoms, corresponding to the narrowing limit.

In Table 4 are given the values of T_1 for the sample OM4. It has three methylene carbon atoms (with i = 2–4) and is a mixture of the four stereoisomers (*mm*, *mr*, *rm*, and *rr*), so that the number of peaks we are concerned with it twelve. We have identified each peak of the ^{13}C NMR spectra by the use of the assignments previously determined for the same sample.[18] However, the intensities of the three peaks associated with the stereoisomer *mm* are very weak, and therefore we have not evaluated their T_1.

For the sample OM5, which is a mixture of the eight stereoisomers, its ^{13}C NMR spectra are rather complicated (see Figure 5 of ref 18) and therefore the individual assignments of the peaks associated with the methylene carbon atoms had not been made in the previous work. Thus we have identified only the four peaks associated with the methylene ^{13}C atoms with i = 2–5 for the stereoisomer *rrr*, which are the strongest of those for the eight stereoisomers, and the results for their T_1 are given in Table 5.

For the samples OM76 and MM2a, the peaks of the ^{13}C NMR spectra associated with the methylene carbon

Table 5. Values of T_1 for OM5 in Acetonitrile at 44 °C

$$\overset{1}{H}CH_2CCH_3(X)\overset{2}{C}H_2CCH_3(X)\overset{3}{C}H_2CCH_3(X)\overset{4}{C}H_2CCH_3(X)-\overset{5}{C}H_2CCH_3(X)H$$

(X = $COOCH_3$)

carbon atom no.	T_1, s	
	c = 0.080 g/cm^3	c = 0.130 g/cm^3
2	0.900	0.830
3	0.824	0.719
4	0.853	0.748
5	0.891	0.809

Table 6. Values of T_1 and NOE for OM76 and MM2a in Acetonitrile at 44 °C

sample	c, g/cm^3	T_1, s	NOE
OM76	0.069	0.13_4	
	0.099	0.13_7	
	0.077		1.5_8
MM2a	0.051	0.12_8	
	0.111	0.12_7	
	0.055		1.6_3

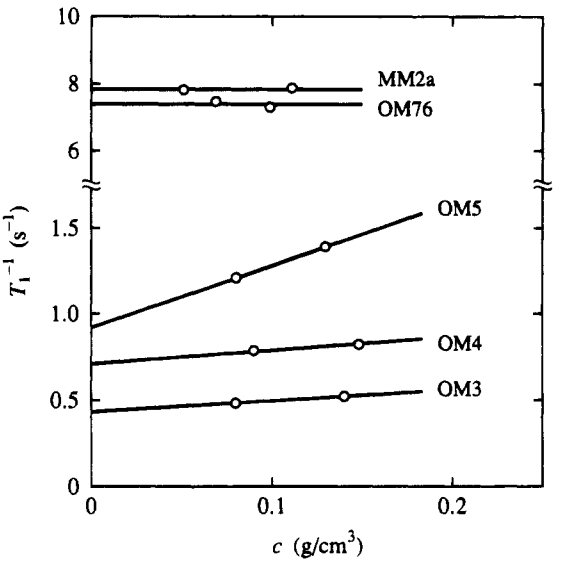

Figure 7. Plots of T_1^{-1} of ^{13}C against c for samples OM3, OM4, OM5, OM76, and MM2a in acetonitrile at 44 °C.

atoms have been identified only for the three kinds of tetrads *mrr*, *rmr*, and *rrr* by the use of the assignments determined by Inoue et al.[19] The average values of T_1 and NOE for these stereoisomers are given in Table 6.

Now, for the samples OM3 and OM4, it is seen from Tables 3 and 4 that T_1 of a given ^{13}C atom depends somewhat on the stereoregularity, as is natural. However, since we are interested in their dependences on M_w, we ignore the minor differences in their values between the stereoisomers and simply consider only their mean values for each methylene ^{13}C atom. Further, since we are interested in the motions of the center (or intermediate) part of the a-PMMA chain, we consider the (mean) value of T_1 of the methylene ^{13}C atom with i = 2 for OM3 and the value averaged over the two (mean) values of T_1 of those with i = 2 and 3 for OM4. Similarly, for OM5, we consider the value of T_1 of the methylene ^{13}C atom with i = 3. We note that, for the samples OM76 and MM2a, the results obtained are just for the intermediate methylene ^{13}C atoms. Figure 7 shows plots of the reciprocal of the (mean) T_1 of the (center) ^{13}C atoms against c for the samples OM3, OM4,

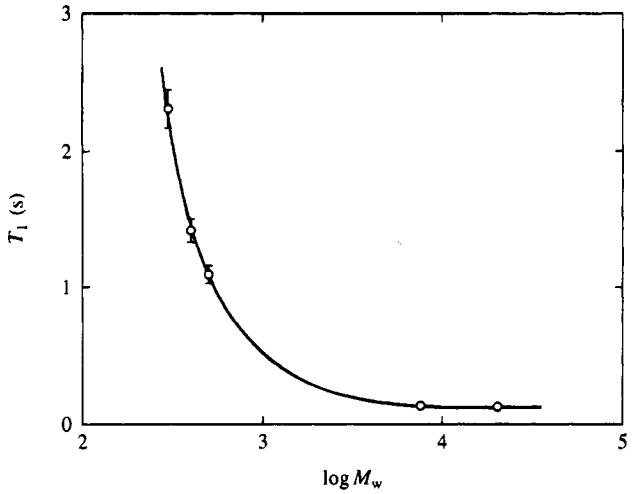

Figure 8. Plots of T_1 of ^{13}C at infinite dilution against the logarithm of M_w for a-PMMA in acetonitrile at 44 °C. The solid curve connects the data points smoothly.

Table 7. Values of T_1 for Atactic Oligo- and Poly(methyl methacrylate)s in Acetonitrile at 44 °C at Infinite Dilution

sample	T_1, s
OM3	2.3_1
OM4	1.4_1
OM5	1.0_9
OM76	0.13_5
MM2a	0.12_8

OM5, OM76, and MM2a. Extrapolation is made to infinite dilution from a pair of data at two concentrations for each sample, following the straight line indicated. The dependence of T_1^{-1} on c is seen to be much larger for the sample OM5 than for the other samples. The same tendency has been observed also for the pentamer (OS5) of a-PS,[1] for which the dependence of T_1^{-1} on c for the center and initiating-end methine ^{13}C atoms is larger than that for the other a-PS samples. The reason for this is not clear.

The values of T_1 thus evaluated at infinite dilution are summarized in Table 7. Note that, for flexible polymer chains, T_1 in general increases with decreasing relaxation time of the orientation of the C–H internuclear vector. Figure 8 shows plots of T_1 thus evaluated at infinite dilution against the logarithm of M_w. The solid curve connects the data points smoothly. The vertical line segments attached to the data points indicate the limit of experimental error, which is due to the ambiguity in the evaluation of T_1 mentioned above. It is seen that T_1 decreases rapidly with increasing M_w for the oligomer samples and reaches its asymptotic value of ca. 0.13 s at $M_w \simeq 10^4$. This dependence of T_1 on M_w is similar to that for the center methine carbon atom of a-PS previously observed[1] and is also consistent with the present results for τ_Γ given in the last subsection.

Discussion

HW Theory. In order to make a comparison of the present results of depolarized LS and nuclear magnetic relaxation measurements with the HW theory in the subsections that follow, it is convenient to here briefly summarize the theoretical results for J_Γ, T_1, and NOE.

For the single (discrete) HW chain composed of N identical rigid subbodies, the power spectrum $J_\Gamma(\Delta\omega)$ of the depolarized component of light scattered from it may be written in the form[4]

$$J_\Gamma(\Delta\omega) = \sum_{k\ \mathrm{odd}} \sum_{j=-2}^{2} A_k^j \frac{\tau_{2,k}^j}{1 + (\Delta\omega\ \tau_{2,k}^j)^2} \tag{12}$$

where

$$\tau_{2,k}^j = 1/\lambda_{2,k}^j \tag{13}$$

$$A_k^j = \frac{12\pi}{N+1} B_k^j \cot^2\left[\frac{\pi k}{2(N+1)}\right] \tag{14}$$

with

$$B_k^j = (8\pi^2)^{-1} \left| \sum_{j'=-2}^{2} \alpha_2^{j'} R_{2,k}^{ij'} \right|^2 \tag{15}$$

In eq 12, $\lambda_{2,k}^j$ are the eigenvalues of the matrix representation of the diffusion operator associated with the subspace spanned by the basis set with the "total angular momentum quantum number" $L = 2$ and the number of "excited" subbodies $n = 1$. Precisely, $J_\Gamma(\Delta\omega)$ is the Fourier–Laplace transform of a linear combination of the basic time-correlation functions associated with that subspace. We use the augmented eigenvalues $\lambda_{2,k}^j$ given by eq 25 of ref 6 (or eq 49 of ref 4) which takes partly into account the interactions with the complementary subspace. Thus $\lambda_{2,k}^j$ may readily be calculated for given values of N and the six model parameters. They are the constant differential-geometrical curvature κ_0 and torsion τ_0 of the characteristic helix, the static stiffness parameter λ^{-1}, the bond length a, and the translational and rotatory friction coefficients ζ_t and ζ_r of the subbody. In eq 15, α_2^j are the spherical tensor components of the polarizability tensor affixed to the subbody, and $R_{2,k}^{ij'}$ is the transformation matrix associated with the eigenvalue problem of the above-mentioned matrix and is given by eq 40 of ref 4. We note that $R_{2,k}^{ij'}$ depends on the parameters κ_0, τ_0, and λ^{-1}.

We assume that the nuclear magnetic spin relaxes due to the heteronuclear dipolar interaction between two unlike spins I and S, with spin I observed and spin S irradiated and with the internuclear distance r between I and S. Then T_1 and NOE for the HW chain introduced above may be given by[5]

$$T_1^{-1} = (1/20)K^2 r^{-6}[J_0(\omega_S - \omega_I) + 3J_1(\omega_I) + 6J_2(\omega_S + \omega_I)] \tag{16}$$

$$\mathrm{NOE} = 1 + \frac{\gamma_S}{\gamma_I}\left[\frac{6J_2(\omega_S + \omega_I) - J_0(\omega_S - \omega_I)}{J_0(\omega_S - \omega_I) + 3J_1(\omega_I) + 6J_2(\omega_S + \omega_I)}\right] \tag{17}$$

where

$$K = \hbar\gamma_I\gamma_S \tag{18}$$

$$J_m(\omega) = 2\sum_{k=1}^{N} (Q_{pk}^0)^2 \sum_{j=-2}^{2} \frac{A_{2,k}^j \tau_{2,k}^j}{1 + (\omega\tau_{2,k}^j)^2} \tag{19}$$

with

$$Q_{pk}^0 = [2/(N+1)]^{1/2} \sin[\pi pk/(N+1)] \tag{20}$$

and with $\tau_{2,k}^j$ and $A_{2,k}^j$ being given by eq 13 and eq 26 of

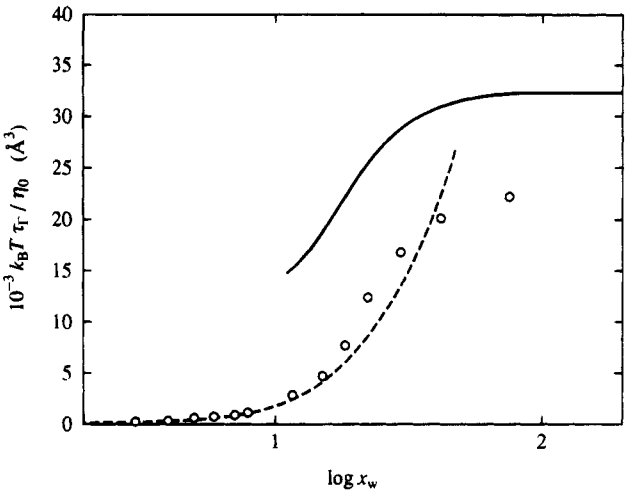

Figure 9. Plots of $k_BT\tau_\Gamma/\eta_0$ against the logarithm of x_w for a-PMMA in acetonitrile at 44.0 °C. The solid and dashed curves represent the theoretical values for the HW model and the rigid sphere model, respectively.

ref 5, respectively. In the above expressions, $\hbar$ is Dirac's constant (Planck's constant divided by 2π), γ_I and γ_S are the gyromagnetic ratios of spins I and S, respectively, and ω_I and ω_S are the respective Larmor angular frequencies. Note that I and S are ^{13}C and ^1H, respectively, in the present case, so that $I = S = 1/2$. In eq 19, the index p indicates the subbody number.

Dependence of τ_Γ on x_w. Now we proceed to make a comparison of the present data for τ_Γ with the HW theory. Figure 9 shows plots of $k_BT\tau_\Gamma/\eta_0$ against the logarithm of x_w for a-PMMA in acetonitrile at 44.0 °C. The solid curve represents the HW theoretical values for τ_Γ as the reciprocal of the hwhm of J_Γ calculated from eqs 12–15 with the values of the (static) model parameters, i.e., $\lambda^{-1}\kappa_0 = 4.0$, $\lambda^{-1}\tau_0 = 1.1$, $\lambda^{-1} = 57.9$ Å, and $\lambda a = 0.048$ ($a = 2.78$ Å),[8,20] those of the (dynamic) parameters, i.e., $\tau_1 \equiv \zeta_t/3\pi\eta_0 a = 1.0$ and $r_2 \equiv \zeta_t/a^2\zeta_r = 8.0$, and those of the Cartesian components of the polarizability tensor α of the subbody given by[4,12]

$$\alpha = \text{diag}(0.581, 0.712, -1.293)\ \text{Å}^3 \quad \text{(a-PMMA)} \quad (21)$$

which is expressed in the localized coordinate system affixed to the subbody and is independent of the subbody number p. We note that the above value of λa has been evaluated from eq 22 of ref 20 with the value 0.0476 of $\lambda\Delta s = \lambda M_0/M_L$, where M_0 is the molecular weight of the repeat unit and is taken to be 100 for a-PMMA, and M_L is the shift factor as defined as the molecular weight per unit contour length and has been determined to be 36.3 Å^{-1} for a-PMMA.[8] We also note that the number N of subbodies in the chain has been set equal to x_w.

The above calculation of the theoretical values requires some remarks. Among the above parameters, only r_2 has been treated as an adjustable one. It has been found that the theoretical asymptotic value of $k_BT\tau_\Gamma/\eta_0$ in the limit of $x_w \to \infty$ becomes a minimum at $r_2 \simeq 13$ and is rather insensitive to the change in r_2 around $r_2 \simeq 13$. Thus we have chosen the above value 8.0 of r_2 so that the theoretical values may reproduce qualitatively the sharp decrease of the experimental values with decreasing x_w. The other dynamic parameter r_1 may also be regarded as adjustable. Then, the agreement between theory and experiment becomes better if a value smaller than unity is assigned to r_1. For convenience, however, we have fixed r_1 to unity as in our previous study of the dynamics of the HW chain.

In Figure 9, we have omitted the theoretical values for $x_w \lesssim 10$, since the block-diagonal approximation[21] adopted in our theory breaks down in the range of such small N. It is seen that the theory may explain semiquantitatively the dependence of $k_BT\tau_\Gamma/\eta_0$ on x_w, although the agreement between theory and experiment is not so good as in the case of a-PS. The theoretical asymptotic value of $k_BT\tau_\Gamma/\eta_0$ in the limit of $x_w \to \infty$ is 3.22×10^4 Å^3 and is ca. 45% larger than the experimental value of ca. 2.2×10^4 Å^3. If we assume as in the previous study[1] that the subbody is an oblate spheroid having the rotation axis of length a and the diameter d, then d is calculated to be equal to 10 Å from eqs 35–38 of ref 22 with the above values of a, r_1, and r_2. This value of d is rather in good agreement with the value 9 Å previously[6] estimated from the chemical structure of a-PMMA.

As in the previous study of a-PS,[1] we consider τ_Γ of the rigid sphere model having the radius equal to the apparent root-mean-square radius of gyration $\langle S^2\rangle_s^{1/2}$ of the HW chain and having a cylindrically symmetric polarizability tensor. It may be given by

$$\tau_\Gamma = 4\pi\eta_0\langle S^2\rangle_s^{3/2}/3k_BT \quad (22)$$

Recall that $\langle S^2\rangle_s$ is defined as the coefficient of the squared scattering vector k^2 in the expansion of the scattering function determined from small-angle X-ray scattering measurements and may be regarded as the mean-square radius of gyration of the excess electron density. Thus it may be given by

$$\langle S^2\rangle_s = \langle S^2\rangle + S_c^2 \quad (23)$$

where $\langle S^2\rangle$ is the (usual) mean-square radius of gyration of the HW chain contour of total length L and is given by

$$\langle S^2\rangle = \lambda^{-2} f_S(\lambda L;\lambda^{-1}\kappa_0,\lambda^{-1}\tau_0) \quad (24)$$

and S_c is the (effective) radius of gyration of the cross section of the excess electron density distributed around the chain contour and has already been evaluated to be $8.4^{1/2}$ Å for a-PMMA.[8] In eq 24, the function f_S is defined by

$$f_S(L;\kappa_0,\tau_0) = \frac{\tau_0^2}{\nu^2} f_{S,KP}(L) + \frac{\kappa_0^2}{\nu^2}\left[\frac{L}{3r}\cos\phi - \frac{1}{r^2}\cos(2\phi) + \frac{2}{r^3 L}\cos(3\phi) - \frac{2}{r^4 L^2}\cos(4\phi) + \frac{2}{r^4 L^2}e^{-2L}\cos(\nu L + 4\phi)\right] \quad (25)$$

with

$$\nu = (\kappa_0^2 + \tau_0^2)^{1/2} \quad (26)$$

$$r = (4 + \nu^2)^{1/2} \quad (27)$$

$$\phi = \cos^{-1}(2/r) \quad (28)$$

and with $f_{S,KP}$ being the function f_S for the Kratky–Porod wormlike chain[22] and given by

$$f_{S,KP}(L) = \frac{L}{6} - \frac{1}{4} + \frac{1}{4L} - \frac{1}{8L^2}(1 - e^{-2L}) \quad (29)$$

The values of τ_Γ calculated from eq 22 with eqs 23–29 are represented by the dashed curve in Figure 9. We

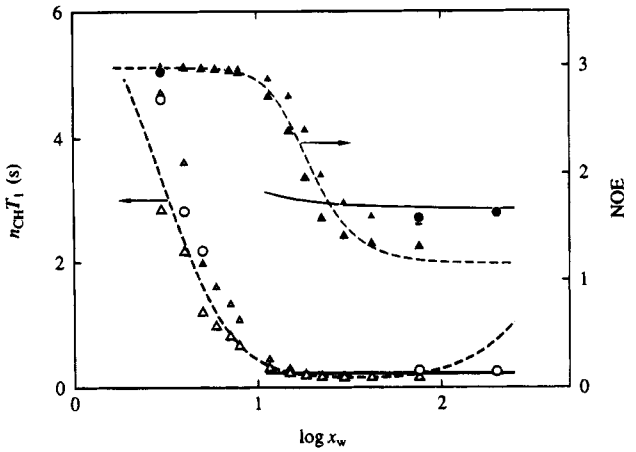

Figure 10. Plots of $n_{CH}T_1$ and NOE of ^{13}C against the logarithm of x_w for the center methylene carbon atoms for a-PMMA in acetonitrile at 44 °C (with $n_{CH} = 2$): (○) $n_{CH}T_1$; (●) NOE. The solid and dashed curves represent the theoretical values for the HW model and the rigid sphere model, respectively. The unfilled and filled large triangles represent the values of $n_{CH}T_1$ and NOE, respectively, calculated with $\tau_M = C\tau_\Gamma$ along with $C = 1$, and the small ones represent those with $C = 0.6$ (see text).

note that the contour length L of the HW chain has been converted to x_w by the use of the relation $x_w = M_L L/M_0$. The dashed curve may reproduce satisfactorily the data points for $x_w \lesssim 10$ as in the case of a-PS. In the latter case, the theoretical values for the rigid sphere model are always larger than the observed ones for $x_w \gtrsim 10$, while for a-PMMA the former values are appreciably smaller than the latter for $20 \lesssim x_w \lesssim 30$. The latter result may be regarded as arising from the fact that the a-PMMA chain, which has rather large λ^{-1}, takes an extended form in such a region (for $x_w \lesssim 30$) and therefore cannot be represented by a rigid sphere.

Dependence of T_1 and NOE on x_w. We make an analysis of the present results for T_1 and NOE along the same line as in the last subsection. Figure 10 shows plots of $n_{CH}T_1$ and NOE of the center methylene ^{13}C atoms against the logarithm of x_w for a-PMMA in acetonitrile at 44 °C, where n_{CH} is the number of C−H bonds attached to the ^{13}C atom under observation and is equal to 2 in the present case. The unfilled and filled circles represent the observed values of T_1 and NOE, respectively, and the solid curves represent the respective HW theoretical values calculated from eqs 16−20 with the same set of values of the static and dynamic model parameters as used in the last subsection. For the calculation of the theoretical values of T_1 and NOE, we must specify the direction (α, β) of the C−H internuclear vector in the localized coordinate system, which is necessary for the calculation of the coefficients $A^j_{2,k}$ in eq 19. The values 90 and ±55° have been adopted as before[5] for the angles α and β in eq 26 of ref 6, respectively. We note that the coefficients $A^j_{2,k}$ in eq 19 and therefore J_m given by eq 19 do not depend on the sign of β when $\alpha = 90°$. This means that the two protons of the two bonded hydrogen atoms make equivalent contributions to T_1, and then T_1 calculated from eqs 16−20 with $\beta = 55°$ is just twice the observed T_1 and therefore is equal to the observed $n_{CH}T_1$. For the Larmor angular frequencies ω_I and ω_S, we have used the values $2\pi \times 100.4 \times 10^6$ and $2\pi \times 399.2 \times 10^6$ rad/s, respectively, corresponding to our measurements. Further, we have adopted the value 1.09 Å of r. The calculation of the theoretical values has been limited again to the range of N (=x_w) $\gtrsim 10$. For such large N, the values of T_1 and NOE observed for the center (intermediate) methylene carbon atoms are actually the mean values averaged over the position of ^{13}C, as noted above, so that we have presented the theoretical values averaged over p.

The HW theoretical values of both $n_{CH}T_1$ and NOE are almost independent of x_w (for $x_w \gtrsim 10$). Their asymptotic values in the limit of $x_w \to \infty$ are 0.223 s and 1.67, respectively, which are in good agreement with the values 0.25_6 s and 1.6_3, respectively, observed for the sample MM2a. This is in contrast to the case of a-PS, for which the HW theory cannot give a good explanation of NOE.

As in the case of J_Γ, we next consider the rigid sphere model having the radius $\langle S^2\rangle_s^{1/2}$, to which a C−H internuclear vector is affixed. T_1 and NOE may then be given by eqs 16 and 17 with J_m given by[23]

$$J_m(\omega) = \frac{2\tau_M}{1 + (\omega\tau_M)^2} \tag{30}$$

where τ_M is identical with τ_Γ given by eq 22. Note that T_1 thus obtained corresponds to the observed $n_{CH}T_1$ as in the case of the HW theoretical values above. In Figure 10, the values of $n_{CH}T_1$ and NOE thus calculated from eqs 16 and 17, respectively, with eq 30 and with the above values of ω_I, ω_S, r, and η_0 are represented by the respective dashed curves. Roughly, the dashed curve for T_1 may explain semiquantitatively the data points for the samples OM3, OM4, and OM5 as well as for τ_Γ. Precisely, however, the differences between the observed and calculated values of T_1 for them are not very small. This disagreement implies that T_1 cannot be explained in terms of the single relaxation time τ_Γ for a-PMMA (with a given M_w) in contrast to the case of a-PS, while this is possible for J_Γ for both polymers.

In order to make the situation clearer, we calculate T_1 and NOE from eqs 16 and 17 with eq 30, where we equate τ_M to the *observed* τ_Γ. If T_1 and NOE could be explained in terms of this τ_Γ, their calculated values would agree well with the observed ones. The values of $n_{CH}T_1$ and NOE thus calculated for all the samples are represented by the unfilled and filled large triangles, respectively, in Figure 10. Except for the value (≃3) of NOE in the narrowing limit, the calculated values (large triangles) are appreciably smaller than the observed ones (circles) in contrast to the case of a-PS.

However, the difference in the situation between a-PMMA and a-PS seems rather natural if it is considered on the basis of the HW theory. As already mentioned, J_Γ may be written in terms of a single relaxation time, i.e., the reciprocal of the eigenvalue $\lambda^j_{2,k}$ with $k = 1$ for a certain branch j ($j = -1$ for a-PMMA and $j = 0$ for a-PS).[4] On the other hand, all the eigenvalues (with all j and k) contribute to T_1 and NOE and there are differences in relative weights of their contributions between a-PMMA and a-PS.[5] Thus we may consider that an *effective* mean (single) relaxation time τ_M, if any, associated with the nuclear magnetic relaxation is very close to τ_Γ for a-PS (as previously shown[1]) but not for a-PMMA. It is then interesting to find that τ_M may be approximately given by

$$\tau_M = C\tau_\Gamma \tag{31}$$

where C is a constant independent of M. If we use,

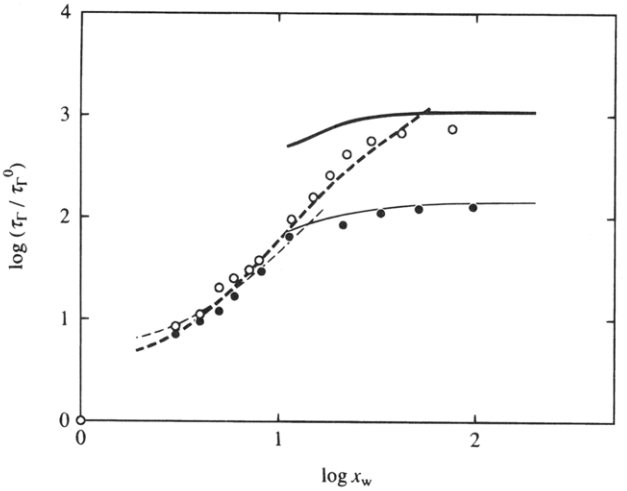

Figure 11. Double-logarithmic plots of $\tau_\Gamma/\tau_\Gamma^0$ against x_w, where τ_Γ^0 is the τ_Γ of the isolated monomer: (○) present data for a-PMMA in acetonitrile at 44.0 °C; (●) previous data for a-PS in cyclohexane at 34.5 °C.[1] The solid and dashed curves represent the theoretical values for the HW model and the rigid sphere model, respectively, with the heavy curves being for a-PMMA and the light ones for a-PS.

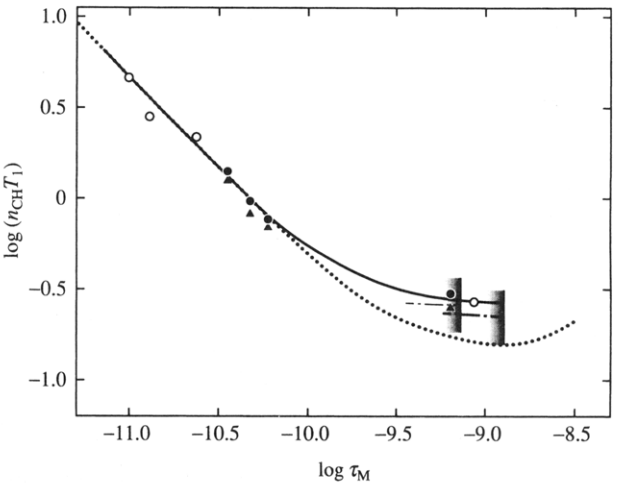

Figure 12. Double-logarithmic plots of $n_{CH}T_1$ (in s) against τ_M (in s): (○) present data for the center methylene ^{13}C atoms for a-PMMA in acetonitrile at 44 °C (with $n_{CH} = 2$); (●) previous data for the center methylene ^{13}C atoms for a-PS in cyclohexane at 40 °C (with $n_{CH} = 2$);[1] (▲) previous data for the center methine ^{13}C atoms for a-PS in cyclohexane at 40 °C (with $n_{CH} = 1$).[1] The heavy and light dot–dashed curves represent the HW theoretical values for a-PMMA and a-PS, respectively, the dotted curve represents the theoretical values for the rigid sphere model, and the solid curve connects the data points smoothly (see text).

instead of $\tau_M = \tau_\Gamma$, eq 31 with $C = 0.6$ (and with the observed τ_Γ) in eq 30, we obtain the values of $n_{CH}T_1$ and NOE represented by the unfilled and filled small triangles instead of the large triangles in Figure 10. These recalculated values are seen to agree well with the observed ones except for T_1 at large x_w, for which the former values are still ca. 40% smaller than the latter. As for a-PS, we note that $C \simeq 1$ (as previously found) and then that the corresponding calculated values of T_1 at large x_w are ca. 30% smaller than the observed ones.

Comparison with a-PS. Finally, in this subsection, we compare the present results for a-PMMA with the previous ones for a-PS.[1] Figure 11 shows double-logarithmic plots of $\tau_\Gamma/\tau_\Gamma^0$ against x_w for a-PMMA in acetonitrile at 44.0 °C (Θ) (unfilled circles) and a-PS in cyclohexane at 34.5 °C (Θ) (filled circles), where τ_Γ^0 is the τ_Γ of the monomer (isolated repeat unit), i.e., $\tau_\Gamma^0 = 0.0019_3$ ns for that of a-PMMA (MIB) and $\tau_\Gamma^0 = 0.0056_2$ ns for that of a-PS (cumene).[1] We note that the values of the reduced relaxation time $k_BT\tau_\Gamma^0/\eta_0$ are $29._6$ and $31._1$ Å^3 for MIB and cumene, respectively, and are in good agreement with each other. The asymptotic value $\tau_{\Gamma,\infty}/\tau_\Gamma^0$ of the ratio $\tau_\Gamma/\tau_\Gamma^0$ in the limit of $x_w \to \infty$ represents the degree of restriction on the rotatory motion of the isolated motional unit (monomer) due to its incorporation into the long enough polymer chain and may be regarded as a measure of "dynamic chain stiffness" (concerning J_Γ) as discussed in the previous theoretical study.[6] The solid and dashed curves represent the theoretical values of τ_Γ divided by the observed ones of τ_Γ^0 for the HW model and the rigid sphere model, respectively.

Although the values of the ratio $\tau_\Gamma/\tau_\Gamma^0$ for a-PMMA and a-PS are close to each other in the oligomer region with very small x_w, the former values become appreciably larger than the latter with increasing x_w. In the limit of $x_w \to \infty$, the ratio of the dynamic chain stiffness $\tau_{\Gamma,\infty}/\tau_\Gamma^0$ of a-PMMA to that of a-PS is found to be 5.8. This confirms our previous conclusion[6] that there is good correlation between dynamic and static chain stiffness. (A theoretical explanation of this correlation has been given in ref 6.) The theoretical value of this ratio is 7.6 and is rather in good agreement with its observed value above. Considering the fact that the HW theoretical values have been calculated by the use of the values of the model parameters determined from analyses of the equilibrium properties along with the proper values of the dynamic parameters, it may be concluded that the dynamic HW theory may explain well the difference in $\tau_{\Gamma,\infty}/\tau_\Gamma^0$ between a-PMMA and a-PS, although the agreement between theory and experiment for the former is only semiquantitative.

In order to examine the relation between T_1 and τ_M, the values of $n_{CH}T_1$ (in s) are plotted double-logarithmically against τ_M (in s) in Figure 12 for the center methylene ^{13}C atoms for a-PMMA in acetonitrile at 44 °C (unfilled circles), for the center methylene ^{13}C atoms for a-PS in cyclohexane at 40 °C (filled circles), and for the center methine ^{13}C atoms for a-PS in cyclohexane at 40 °C (filled triangles), where the values of τ_M have been calculated from eq 31 with the observed values of τ_Γ and with $C = 0.6$ and 1 for a-PMMA and a-PS, respectively. Although the values of T_1 for the methylene ^{13}C atoms for a-PS at infinite dilution were not evaluated in the previous paper, we have evaluated them in the same manner as mentioned in the Results section. Further, for a-PS (in cyclohexane at 40 °C), we have used the values of the scaled τ_Γ (i.e., τ_Γ*) evaluated in the previous paper.[1] The heavy and light dot–dashed curves represent the HW theoretical values calculated for a-PMMA and a-PS, respectively, in the same manner as in the previous subsection. The right-end point of each curve bounded by the vertical line segment with the shade corresponds to the asymptotic value of τ_Γ in the limit of $x_w \to \infty$, and the other end point corresponds to $x_w = 10$. The dotted curve represents the values calculated for the rigid sphere model from eq 16 with eq 30. Note that in the figure the data for both the center methylene and methine ^{13}C atoms for a-PS have been plotted in order to show explicitly the difference in T_1 between them mentioned in the previous paper.[1] However, this difference is seen to be rather minor, and

therefore we ignore it here. It is seen that the data points for a-PMMA and a-PS form nearly a single-composite curve as shown by the solid curve, and follow the dotted curve for small τ_M (for $\log n_{CH}T_1 \gtrsim -0.2$), as was expected. Naturally, the data do not give a single-composite curve for small τ_M when plotted against $\log \tau_\Gamma$ as in the previous paper,[1] since the values of C for a-PMMA and a-PS are different.

Conclusion

The power spectra $J_\Gamma(\Delta\omega)$ of the excess depolarized component of light scattered from a-PMMA in acetonitrile at 44.0 °C (Θ) have been determined accurately despite the fact that there is a difficulty inherent in this polymer–solvent system, i.e., a solution of a solute of small optical anisotropy in a solvent of large one. Then it has been found that $J_\Gamma(\Delta\omega)$ may be well represented in terms of a single Lorentzian independently of x_w for $3 \leq x_w \lesssim 76$ and that the relaxation time τ_Γ as defined as the reciprocal of the hwhm of J_Γ increases with increasing x_w and levels off to its asymptotic value in the limit of $x_w \to \infty$ as in the case of a-PS previously[1] studied. These results are consistent with our recent theoretical prediction on the basis of the HW chain model.[4] A rather detailed analysis of the data shows that the HW theory may explain semiquantitatively the observed dependence of τ_Γ (or J_Γ) on x_w over that range of x_w for which the theory is applicable, i.e., for $x_w \gtrsim 10$, while the rigid sphere model having the radius equal to the apparent root-mean-square radius of gyration $\langle S^2\rangle_s^{1/2}$ of the HW chain, as introduced in the previous paper,[1] may reproduce well the data for $x_w \lesssim 10$ as in the case of a-PS. From a comparison of the present results for a-PMMA with the previous ones for a-PS, it is shown that the dynamic chain stiffness, as previously defined as the ratio of the relaxation time associated with the local motion of a long polymer chain to that of its isolated repeat unit (monomer), is larger for a-PMMA than for a-PS, as was expected, and that this difference may be well explained by the HW theory.

As for the results of nuclear magnetic relaxation measurements, the HW theory can explain them quantitatively for T_1 and also for NOE for $x_w \gtrsim 10$. In contrast to the case of a-PS, the rigid sphere model cannot give a quantitative explanation of T_1 even for $x_w \lesssim 10$, indicating that the dynamic depolarized scattering and nuclear magnetic relaxation cannot be described in terms of a common single relaxation time. However, the (mean) magnetic relaxation time τ_M has been found to be approximately equal to $0.6\tau_\Gamma$, indicating that the relation between τ_Γ and τ_M depends generally on the kind of polymer.

Acknowledgment. This research was supported in part by a Grant-in-Aid (04650809) from the Ministry of Education, Science, and Culture, Japan.

References and Notes

(1) Takaeda, Y.; Yoshizaki, T.; Yamakawa, H. *Macromolecules* **1994**, *27*, 4248.
(2) Yamakawa, H. In *Molecular Conformation and Dynamics of Macromolecules in Condensed Systems*; Nagasawa, M., Ed.; Elsevier: Amsterdam, 1988; p 21.
(3) Yamakawa, H. *Annu. Rev. Phys. Chem.* **1984**, *35*, 23.
(4) Yoshizaki, T.; Yamakawa, H. *J. Chem. Phys.* **1993**, *99*, 9145.
(5) Yamakawa, H.; Fujii, M. *J. Chem. Phys.* **1984**, *81*, 997.
(6) Yamakawa, H.; Yoshizaki, T.; Fujii, M. *J. Chem. Phys.* **1986**, *84*, 4693.
(7) Konishi, T.; Yoshizaki, T.; Shimada, J.; Yamakawa, H. *Macromolecules* **1989**, *22*, 1921 and succeeding papers.
(8) Tamai, Y.; Konishi, T.; Einaga, Y.; Fujii, M.; Yamakawa, H. *Macromolecules* **1990**, *23*, 4067.
(9) Fujii, Y.; Tamai, Y.; Konishi, T.; Yamakawa, H. *Macromolecules* **1991**, *24*, 1608.
(10) Dehara, K.; Yoshizaki, T.; Yamakawa, H. *Macromolecules* **1993**, *26*, 5137.
(11) Abe, F.; Einaga, Y.; Yoshizaki, T.; Yamakawa, H. *Macromolecules* **1993**, *26*, 1884.
(12) Takaeda, Y.; Yoshizaki, T.; Yamakawa, H. *Macromolecules* **1993**, *26*, 3742.
(13) Abe, F.; Horita, K.; Einaga, Y.; Yamakawa, H. *Macromolecules* **1994**, *27*, 725.
(14) Abe, F.; Einaga, Y.; Yamakawa, H. *Macromolecules* **1994**, *27*, 3262.
(15) Yoshizaki, T.; Takaeda, Y.; Yamakawa, H. *Macromolecules* **1993**, *26*, 6891.
(16) Ouano, A. C.; Pecora, R. *Macromolecules* **1980**, *13*, 1167.
(17) Hernandez, G. *Fabry–Perot Interferometers*; Cambridge University Press: Cambridge, 1986.
(18) Konishi, T.; Tamai, Y.; Fujii, M.; Einaga, Y.; Yamakawa, H. *Polym. J.* **1989**, *21*, 329.
(19) Inoue, Y.; Nishioka, A.; Chûjô, R. *Polym. J.* **1971**, *4*, 535.
(20) Yamakawa, H.; Yoshizaki, T. *J. Chem. Phys.* **1981**, *75*, 1016.
(21) Yamakawa, H.; Yoshizaki, T.; Shimada, J. *J. Chem. Phys.* **1983**, *78*, 560.
(22) Kratky, O.; Porod, G. *Recl. Trav. Chim. Pays-Bas* **1949**, *68*, 1106.
(23) Solomon, I. *Phys. Rev.* **1955**, *99*, 559.

MA941085P